Electronic Supplementary Information

One Dimensional $CuInS_2$-ZnS Heterostructured Nanomaterials as Low-Cost and High-Performance Counter Electrodes of Dye-Sensitized Solar Cells

Luoxin Yi,[a] Yuanyuan Liu,[a] Nailiang Yang,[a] Zhiyong Tang,[b] Huijun Zhao,[c] Guanghui Ma,[a] Zhiguo Su,[a] and Dan Wang*,[a]

[a] State Key Laboratory of Biochemical Engineering, State Key Laboratory of Multiphase Complex Systems, Institute of Process Engineering, Chinese Academy of Sciences, Beijing 100190, P. R. China Fax: +86 10 62631141 Tel: +86 10 62533616 E-mail: danwang@mail.ipe.ac.cn

[b] National Center for Nanoscience and Technology, 100190, P. R. China

[c] Centre for Clean Environment and Energy, Gold Coast Campus, Griffith University, Queensland 4222, Australia

Synthesis of $Cu_{1.94}S$ Nanocrystals

$Cu_{1.94}S$ nanocrystals were synthesized in our laboratory, and the synthetic processes were carried out under the protection of nitrogen gas.

The synthesis of spherical $Cu_{1.94}S$ nanocrystals was accomplished by directly decomposing 30 mL dodecanethiol solution containing 0.13 g $Cu(acac)_2$ (0.5 mmol) at the temperature of 200 °C for 1 hours. The resultant solution was dripped into 3-fold ethanol (by volume) to precipitate nanocrystals which were subsequently collected by centrifugation at 4000 rpm for 10 min. The following purification procedures included the redispersion of the nanocrystals in n-hexane (equal volume to the resultant solution) and the collection of the nanocrystals by centrifugation at 4000 rpm for 10 min. The redispersion/centrifugation procedures were repeated twice, and then the resultant nanocrystals were obtained for further synthesis of $CuInS_2$ nanocrystals or redispersed in toluene for characterization.

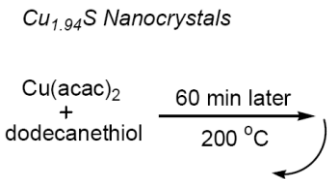

Scheme S1. Synthetic route for preparing $Cu_{1.94}S$ nanocrystals.

Synthesis and Characterization of Matchstick-like $Cu_{1.94}S$–ZnS Heterostructured Nanorods.

$Cu_{1.94}S$–ZnS heterostructure nanorods were also synthesized under the protection of nitrogen gas, and more details of the synthesis and characterizations were published elsewhere.

The matchstick-like $Cu_{1.94}S$–ZnS heterostructure nanocrystals were prepared as follows: 0.13 g $Cu(acac)_2$ (0.5 mmol) was firstly pyrolyzed in 30 mL dodecanethiol at 200 °C. In the meantime, 15 mL dodecanethiol stock solution containing 0.13 g (0.5 mmol) $Zn(acac)_2$ was prepared and divided into six equal portions which were intermittently injected into the hot $Cu(acac)_2$-dodecanethiol solution at 200 °C at fixed time intervals. For example, the first portion was injected after $Cu(acac)_2$ and dodecanethiol reacted for 25 min and the second portion was followed 20 min later. The remaining four injections were finished by each time interval of 60 min. After the last injections, the reaction mixture was maintained at 200 °C for 17 hours and then cool down to room temperature. 15 mL resultant solution was treated by the same purification procedures as those for $Cu_{1.94}S$ nanocrystals, and the $Cu_{1.94}S$–ZnS heterostructured nanorods were obtained in brown precipitate which was used as seed for further synthesis of $CuInS_2$–ZnS heterostructured nanocrystals.

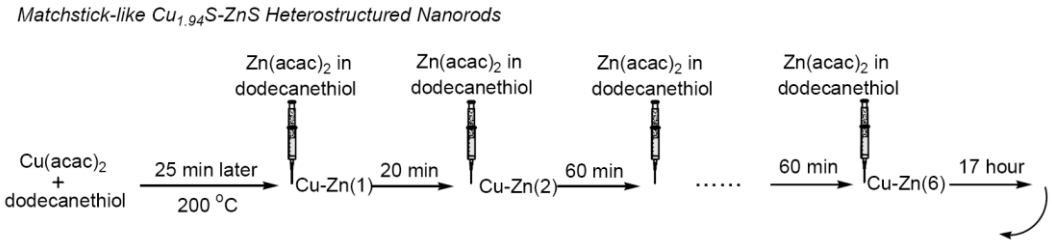

Scheme S2. Synthetic route for preparing $Cu_{1.94}S$–ZnS heterostructured nanorods.

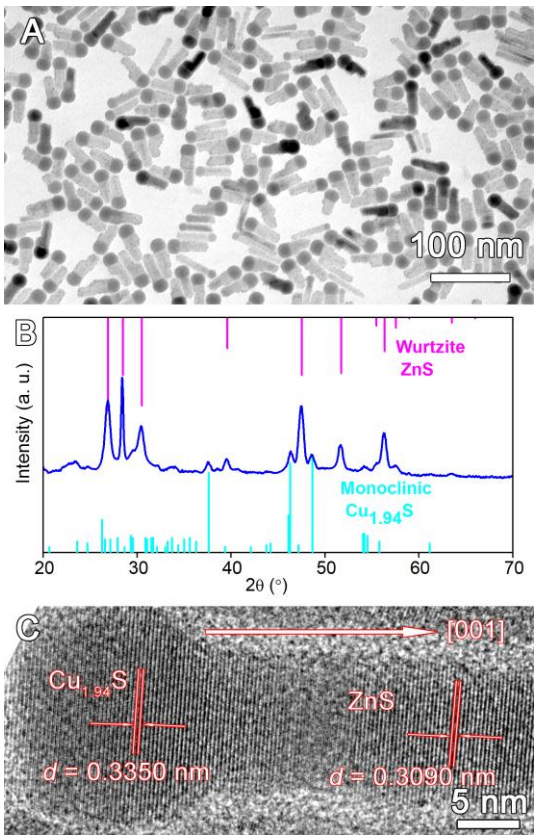

Figure S1. TEM image (A) XRD pattern (B) of $Cu_{1.94}S$–ZnS heterostructured nanorods together with standard diffraction lines of wurtzite ZnS (JCPDS No.79-2204) at top and the lines of monocline $Cu_{1.94}S$ (JCPDS No.23-0959) shown at bottom for comparison; (C) HRTEM image of a single nanorod which shows the crystal spacing for the judgment of the axis direction of the single crystal.

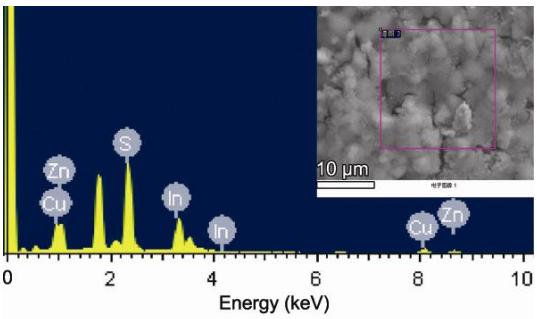

Element	Mass Percentage (%)	Atom Percentage (%)
S K	26.57	48.03
Cu L	18.22	16.62
Zn L	19.64	17.41
In L	35.56	17.95
Total	100.00	100.00

Figure S2. EDS spectrum of BTCIS–ZnS heterostructured nanorods over an area of approximately 20 μm × 20 μm on silicon. The below table lists the ratios of the elements detected by EDS.

Synthesis and Characterization of FCIS Nanocrystals.

100 mg $Cu_{1.94}S$ nanocrystal seeds were redispersed in 10 mL of octadecene. Subsequently, 0.06 g (0.20 mmol) of $In(ac)_3$ and 1.0 mL dodecanethiol were introduced. The reaction was heated to 200 °C with magnetic stirring and kept for 4 hours for generating FCIS nanocrystals (Fig. S3). in which the axial length is 32.7 ± 2.4 and the maximum width is 20.7 ± 1.0 nm.

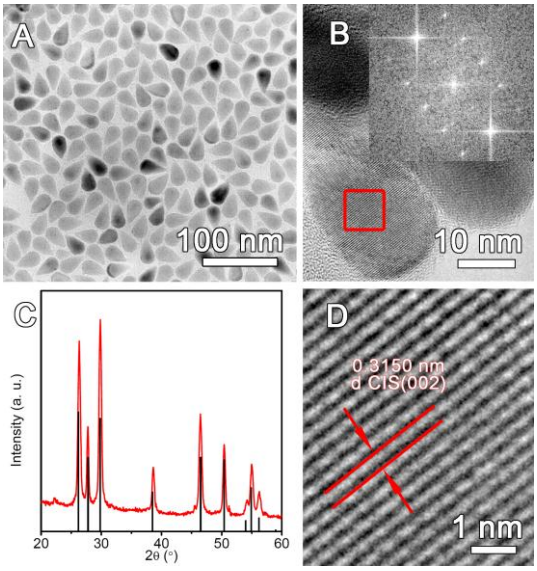

Figure S3. TEM image (A) of FCIS nanocrystals; HRTEM image (B) of single nanocrystal and the inset is the selected area FFT pattern transformed form the red rectangular area; XRD pattern (C) of the nanocrystals together with wurtzite CIS diffraction lines; (D) HRTEM image of the enlarged red rectangular area of (B), showing the crystalline spacing along the axis direction.

Monoclinic $Cu_{1.94}S$ and Cu_2S prefer converting to the hexagonal polymorph (chalcocite: space group P63/mmc, a = 3.985, c =6.806) at the temperature of above 103 °C. On the basis of the standard crystal data of hexagonal Cu_2S and CIS, atomic packing models that depict their {001} and {100} facets are shown in Fig. S5. Close inspection of the {001} and {100} facets discloses that Cu_2S possesses a high density of copper ions sandwiched between every two layers of sulfur anions, giving rise to the large interspaces lack of Cu cations between the two rows of unit cells (top half in Fig. S5). Therefore, such large interspaces could supply the enough space for the indium ions entering along the perpendicular direction to [001] (bottom half in Fig. S5).

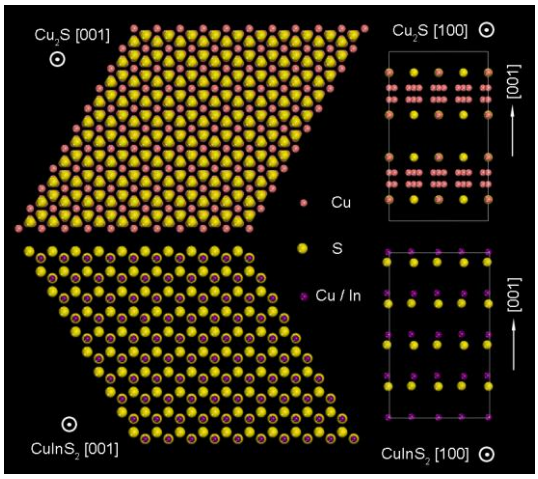

Figure S4. Crystallographic model of the hexagonal high chalcocite structure of Cu_2S (top) and WZ–CIS (bottom) viewed from the [001] (left) and [100] (right) direction for depicting the arrangement of the atoms of {001} facets and {100}.

To answer the question that why both spherical $Cu_{1.94}S$ nanocrsytals and semi-spherical $Cu_{1.94}S$ heads in the $Cu_{1.94}S$–ZnS heterostructures are changed into flame-like CIS nanocrystals after addition of indium precursors, the evolution of FCIS nanocrystals was studied. Two termediate products, which were obtained at 0 h and 0.5 h after 200 °C, were respectively named as the intermediate nanocrystals I and intermediate nanocrystals II. As shown in Fig. S4A, the initial nanocrystal seeds of 15.1 ± 1.2 nm are spherical, and XRD shows that they are composed of monoclinic $Cu_{1.94}S$ nanocrystals. After heating from room temperature to 200 °C within 8 min by using the octadecene mixture solvent containing dodecanethiol as ligand and $In(ac)_3$ as indium source, the diameters of the intermediate products increase to 16.8 ± 1.4 nm (Fig. S4B). More interestingly, the nanocrystals at this stage are mainly monoclinic Cu_2S with a minor amount of CIS. The coexistence of Cu_2S and CIS phases indicates that increasing the reaction temperature and gradual incorporation of indium ions cause the transformation of monoclinic $Cu_{1.94}S$ to Cu_2S, meanwhile CIS starts to be formed. Since all the CIS in Fig. S4B have uniform sizes, we can conclude that CIS should be produced inside the original nanocrystal matrix rather than formation as the new particles. After 0.5 h reaction at 200 °C, the quasi-flame-shaped particles that are assigned to WZ–CIS are clearly identified (Fig. S4C), and only small portion of Cu_2S phase is left according to the XRD measurements.

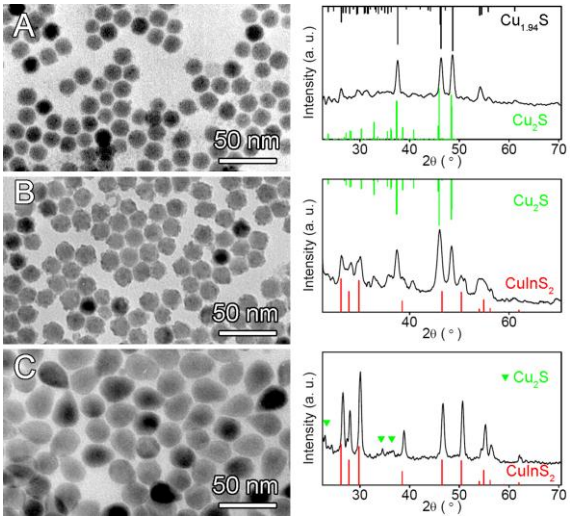

Figure S5. TEM image of $Cu_{1.94}S$ seeds (A) and XRD patterns laid aside with the standard diffraction peaks of $Cu_{1.94}S$ (JCPDS card 23–0959) and Cu_2S (JCPDS card 73–1138) for comparison. TEM images and XRD patterns of intermediate nanocrystals obtained after 0 h (B) and 0.5 h (C) reaction at 200 °C. The corresponding comparison of Cu_2S and CIS is also given at the top and bottom in each XRD frames.

Photovoltaic Devices Constructed with BTCIS-ZnS Nanocrystals

Table S1: Photovoltaic performances of DSSCs using BTCIS–ZnS with different thicknesses as the counter electrodes (*T*)

T (μm)	J_{SC} (mA cm^{-2})	V_{OC} (V)	*FF* (%)	η (%)
2.0	11.8	0.77	67.1	6.1
1.0	12.6	0.77	67.1	6.5
0.8	14.1	0.76	67.2	7.2
0.5	10.4	0.76	67.0	5.3

J_{SC} = short-circuit current density; V_{OC} = open-circuit voltage; FF = fill factor; η = power conversion efficiency

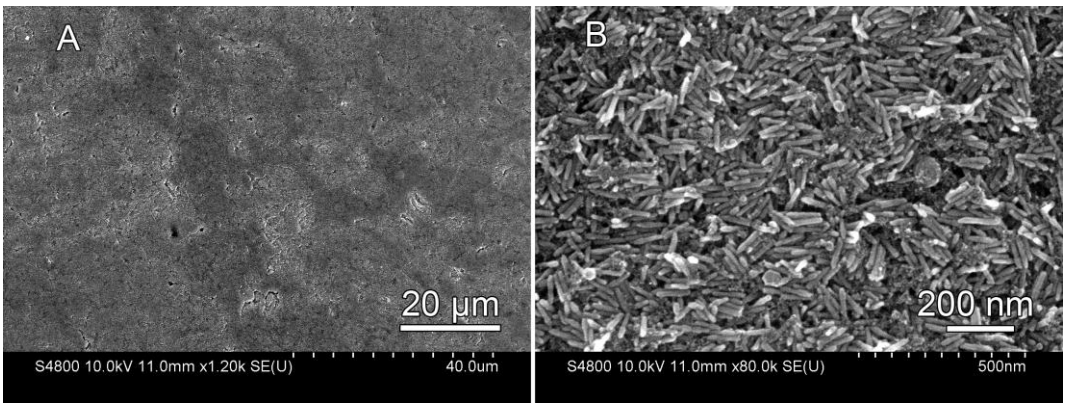

Figure S6. SEM images of LRCIS–ZnS film drop-cast on FTO-coated glass after sintering at 550 °C under a nitrogen atmosphere for 30 min.

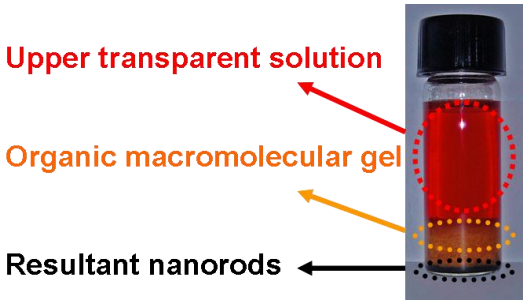

Figure S7. The photograph of the sample vial for burning torch-like $CuInS_2$–ZnS heterostructured nanorods.

It should be mentioned that the $In(ac)_3$ reacted with dodecanethiol to generate a macromolecule gel, which gradually disappeared during the thermal decomposition process. At the same time, along with the formation of the BTCIS–ZnS heterostructured nanorods, the byproduct of fluorescent CIS quantum dots started to appear in the reaction system. Interestingly, the heterostructured nanorod products were produced as the solid precipitates at the bottom layer, the remained gel stayed at the middle layer, and fluorescent CIS quantum dots were dispersed in the supernatant solution, respectively (Fig. S7). The stratified solution made the separation easy, and the structural and spectroscopic characterizations of CIS quantum dots were shown in Fig. S8.

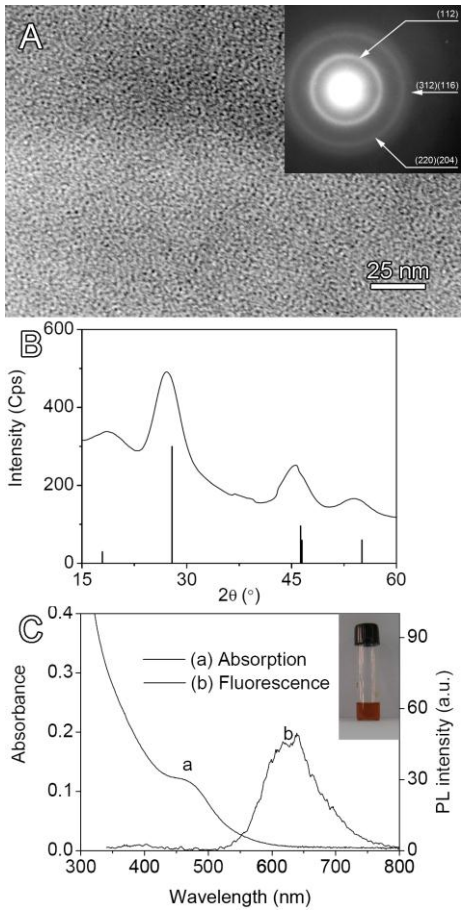

Figure S8. TEM image and SAED (A) of the nanoparticles obtained from the upper transparent solution; XRD pattern (B) of the nanoparticles together with diffraction lines of standard chalcopyrite CIS (JCPDS No. 85-1575) at bottom for comparison; absorption and fluorescence spectra (C) of the nanoparticles in toluene.